

# Robust preparation of ground state phases under noisy imaginary time evolution

Aleksei Khindanov,<sup>1</sup> Yongxin Yao,<sup>1,2</sup> and Thomas Iadecola<sup>1,2,\*</sup>

<sup>1</sup>Ames National Laboratory, U.S. Department of Energy, Ames, Iowa 50011, USA

<sup>2</sup>Department of Physics and Astronomy, Iowa State University, Ames, Iowa 50011, USA

(Dated: June 7, 2024)

Non-unitary state preparation protocols such as imaginary time evolution (ITE) offer substantial advantages relative to unitary ones, including the ability to prepare certain long-range correlated states more efficiently. Here, we ask whether such protocols are also robust to noise arising due to coupling to the environment. We consider a non-unitary ITE “circuit” subjected to a variety of noise models and investigate whether the resulting steady state remains in the same phase as the target state of the ITE at finite noise strength. Taking the one-dimensional quantum Ising model as a concrete example, we find that the ground state order and associated phase transition persist in the presence of noise, provided the noise does not explicitly break the symmetry that protects the phase transition. That is, the noise must possess the protecting symmetry in a weak (or average) form. Our analysis is facilitated by a mapping to an effective Hamiltonian picture in a doubled Hilbert space. We discuss possible implications of these findings for quantum simulation on noisy quantum hardware.

## I. INTRODUCTION

High-caliber ground state preparation is a necessary step for many quantum chemistry and quantum many-body physics algorithms, most notably quantum phase estimation [1–4]. While various approaches to the ground state preparation have been proposed, such as adiabatic [5–7] and variational [8–10] state preparation, many of them suffer from limitations, particularly when being executed on near-term devices where resources for quantum computation are scant. These limitations can include a small energy gap along the adiabatic path, the dependence on a variational ansatz or an ill-behaved classical optimization subroutine.

Another conceptual approach to ground state preparation, which can potentially be more suitable for near-term implementation, is based on imaginary time evolution (ITE) [3, 11–28]. Being a non-unitary operation, the ITE cannot be implemented using only unitary gates; nevertheless, various algorithms have been designed that *effectively* realize an approximate ITE process on a quantum device. These algorithms either (1) perform local tomography to determine a unitary such that the unitarily-evolved state approximates the ITE-evolved state [11–16] (this is known as quantum imaginary time evolution, or QITE), (2) classically construct an adiabatic protocol that emulates the ITE [17] (this is known as adiabatic quantum imaginary time evolution, or A-QITE), (3) take advantage of the variational principle [18–24] (this is known as variational quantum imaginary time evolution, or VQITE), (4) utilize ancilla(e) and measurements [25–27] (this is known as probabilistic imaginary time evolution, or PITE), or (5) ancilla(e), measurements, and feedback [28]. These and other sophisticated protocols become increasingly realizable on present-day

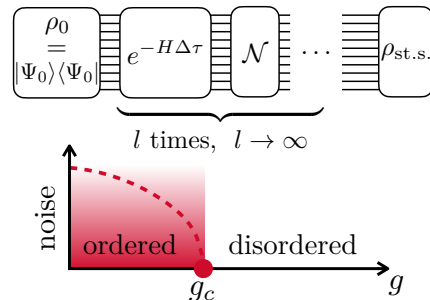


FIG. 1. (Top) Schematic of the model studied in this paper. An initial pure state is fed into a “circuit” consisting of black-box ITE (represented in a Trotterized form) followed by a noise channel  $\mathcal{N}$ . The object of interest is the steady state density matrix obtained upon iterating this evolution. (Bottom) When the Hamiltonian  $H$  has a ground-state phase transition at a parameter  $g = g_c$ , this becomes a dynamical phase transition in the steady state of the ITE circuit in the limit of zero noise. For certain noise channels, it is possible for this phase transition to persist in the presence of noise, giving rise to a two-dimensional phase diagram.

and near-term devices due to rapid hardware advances, such as the ever more efficient implementation of mid-circuit measurements and the adoption of dynamical circuits [29–31].

So far the design of the ITE algorithms has primarily focused on the efficiency of their implementation on near-term machines—the proposed protocols attempt to minimize both the number of qubits required for the algorithm and the number of circuit layers, including measurements. However, another factor that has so far been mostly overlooked in studies of ITE algorithms is their stability to quantum noise arising due to coupling of the system to the environment. In the absence of quantum error correction, the effects of noise are ubiquitous in near-term devices where it generally tends to damage quantum information and corrupt the performance

\* iadecola@iastate.edu

of quantum algorithms [2, 32].

In this work we ask whether ITE-based ground state preparation is robust to various types of noise commonly present in experimental setups. To keep our considerations as general and as simple as possible, we refrain from directly modeling a particular algorithm implementing the ITE, and instead consider a black box realizing a Trotterized version of ITE [33]. A “circuit” constructed in this way can be thought of as a toy model of an ITE protocol, which we further subject to noise (see Fig. 1). Within this model the ITE effectively realizes an approximate (due to the Trotter error) weak projection onto a target ground state, which may belong to a nontrivial phase, whereas noise tends to trivialize the state it acts upon. Here we analyze this competition between ITE and noise by investigating whether the mixed state resulting from the noisy ITE process belongs to the same nontrivial *phase* as the targeted pure ground state. Note that this is different from the conventional task of the quantum state preparation, which amounts to preparing a state that maximizes the overlap with a target state.

As a concrete example, we focus on the one-dimensional transverse-field Ising model whose ground-state quantum phase transition is a prototypical example of long-range order and spontaneous symmetry breaking (SSB). We investigate whether this order, and the quantum critical point from which it emerges, persists in the mixed steady state of the ITE at finite noise strength. To this end, in the limit of infinitesimal imaginary Trotter step we take advantage of the Choi-Jamiołkowski isomorphism [34, 35] and map the noisy ITE of interest to a noiseless ITE under an effective Hamiltonian in a doubled Hilbert space. This allows us to extract the steady state properties of the noisy ITE from the ground state of the effective Hamiltonian, which can be efficiently calculated using the density matrix renormalization group (DMRG) [36–38]. To further corroborate our findings and investigate the effect of imaginary-time Trotter error, we also perform direct simulations of our noisy ITE “circuit” for comparatively small system sizes. We find that the ordered phase is stable to sufficiently weak noise as long as the noise does not explicitly break the weak version [39, 40] of the symmetry that is spontaneously broken at the ground-state quantum critical point. These findings are in contrast to the naive expectation that noise should act similarly to a finite temperature, and thus should destroy any order and criticality in one dimension.

Our study connects to investigations of phases and phase transitions in open quantum systems [41–44]. A growing body of research has focused on defining, characterizing, and designing mixed-state versions of symmetry protected topological (SPT) phases, quantum critical states, and topological order [40, 45–79]. Many of these works specifically describe the fate of these nontrivial phases and states under noisy channels (see, for example, Refs. [50–52]) and employ the doubled Hilbert space formalism in their analyses of mixed states [51–53].

The present work differs in that the ITE tends to counteract the trivializing effect of the noise—heuristically, if the ITE superoperator is gapped, the added noise acts as a perturbation that can only destroy an ordered phase by closing the gap. This brings additional connections to passive error correction [59, 80, 81] and adaptive quantum circuits [82–85].

The rest of this paper is organized as follows. In Sec. II we introduce the model and review the basics of the doubled Hilbert space formalism. We present our main results in Sec. III, focusing on several illustrative examples of both Pauli (Sec. III A) and non-Pauli (Sec. III B) noise channels. We conclude in Sec. IV, where we touch on possible implications of our results for ITE quantum algorithms implemented on noisy hardware.

## II. MODEL

We consider a Trotterized evolution along the imaginary time axis as a black box model for an ITE protocol. Assuming that the target Hamiltonian can be decomposed into a sum of local terms as  $H = \sum_m h_m$ , the mixed-state density matrix  $\rho$  after each Trotter step becomes

$$\mathcal{I}_m[\rho] = \frac{e^{-\Delta\tau h_m} \rho e^{-\Delta\tau h_m}}{\text{Tr}[e^{-2\Delta\tau h_m} \rho]}, \quad (1)$$

where  $\Delta\tau$  is the size of the Trotter step. For small  $\Delta\tau$  the composition of superoperators  $\mathcal{I}_m$ ,

$$\mathcal{I}[\rho] = \prod_m \mathcal{I}_m[\rho], \quad (2)$$

effectively implements a weak projection onto the ground state manifold of  $H$ , as long as the initial state has a nonzero overlap with this subspace.

In this work, as a target Hamiltonian  $H$  we take the familiar one-dimensional transverse-field Ising chain:

$$H = -J \sum_i \sigma_i^z \sigma_{i+1}^z + g \sum_i \sigma_i^x \equiv H_Z + H_X. \quad (3)$$

Here  $J$  sets the overall energy scale and from now on we set  $|J| = 1$ . For both the ferromagnetic ( $J = +1$ ) and the antiferromagnetic ( $J = -1$ ) chain the Hamiltonian (3) possesses a  $\mathbb{Z}_2$  symmetry generated by  $U = \prod_i \sigma_i^x$ , while its ground state exhibits an ordered (disordered) phase for transverse field values  $g < 1$  ( $g > 1$ ) and undergoes an SSB phase transition at the critical point  $g = g_c = 1$ .

In the absence of noise and in the limit of small  $\Delta\tau$ , the steady state of the evolution (1)–(2) exhibits a (dynamical) phase transition inherited from the ground-state phase transition of  $H$ . We now ask whether the ordered phase and the associated phase transition survive in the presence of noise. We describe a noise channel affecting the circuit in terms of its Kraus operators  $K_k$ :

$$\mathcal{N}[\rho] = \sum_k K_k \rho K_k^\dagger, \quad (4)$$

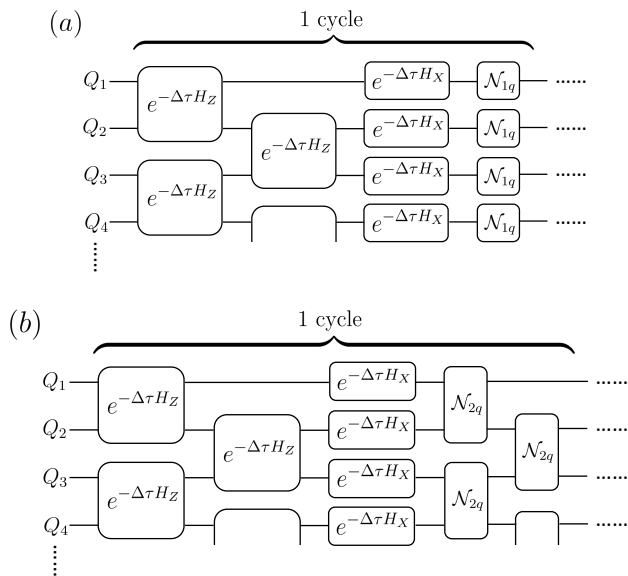


FIG. 2. Schematic depiction of the circuit implementation of the noisy ITE evolution (5) for the transverse-field Ising chain in the case of (a) single-qubit and (b) two-qubit noise. Here  $e^{-\Delta\tau H_Z}$  and  $e^{-\Delta\tau H_X}$  represent the Trotterized ITE parts of the protocol, while  $\mathcal{N}_{1q}$  and  $\mathcal{N}_{2q}$  denote the single- and two-qubit noise, respectively.

where the Kraus operators satisfy the condition  $\sum_k K_k^\dagger K_k = I$  and  $I$  is the identity operator. The specific form of the Kraus operators depends on the type of noise. In this work we consider multiple types of noise: single-qubit bit-flip, depolarizing, and amplitude damping noise, as well as correlated two-qubit bit-flip noise.

The evolution that we investigate can be described as a joint action of the ITE and the noise operations at each Trotter step:

$$\rho_{\text{st.s.}} = \dots \mathcal{N}[\mathcal{I}[\mathcal{N}[\mathcal{I}[\rho_0]]]] \dots \quad (5)$$

Here  $\rho_0$  is some initial state that has a nonzero overlap with the ground state manifold of  $H$ , and the evolution (5) is performed until the steady state  $\rho_{\text{st.s.}}$  is reached. For the Ising chain (3) we schematically depict the ‘‘circuit’’ implementation of one cycle of the evolution (5) in Fig. 2, where Figs. 2(a) and (b) correspond to the cases of one-qubit and two-qubit noise, respectively.

To probe the steady state of the noisy ITE we employ the vectorization technique (also known as the Choi-Jamiołkowski isomorphism [34, 35]), rewriting the density operator  $\rho$  as a state vector in a doubled Hilbert space. We denote this state vector by  $|\rho\rangle\rangle$ , and define it via

$$|\rho\rangle\rangle = \sum_{mn} \rho_{mn} |m\rangle \otimes |n\rangle, \quad (6)$$

where  $\rho_{mn}$  are matrix elements of the density operator  $\rho = \sum_{mn} \rho_{mn} |m\rangle\langle n|$  in the computational basis of the original Hilbert space. Within this formalism, the ITE

superoperator  $\mathcal{I}_m$  of Eq. (1) becomes an operator acting on the doubled space:

$$\tilde{\mathcal{I}}_m \propto e^{-\Delta\tau h_m} \otimes (e^{-\Delta\tau h_m})^*, \quad (7)$$

where we utilize a tilde to denote operators in the doubled space and where we have omitted a  $|\rho\rangle\rangle$ -dependent normalization. The noise superoperator  $\mathcal{N}$  of Eq. (4), in turn, corresponds to an operator

$$\tilde{\mathcal{N}} = \sum_k K_k \otimes K_k^*. \quad (8)$$

Given an (in general unnormalized) density operator  $\rho$ , the mixed state expectation value of an observable  $O$  can be computed within the doubled space formalism as

$$\langle O \rangle = \frac{\text{Tr}[\rho O]}{\text{Tr}[\rho]} = \frac{\langle\langle I|O \otimes I|\rho\rangle\rangle}{\langle\langle I|\rho\rangle\rangle}, \quad (9)$$

where the state vector  $|I\rangle\rangle = \sum_m |m\rangle \otimes |m\rangle$  corresponds (up to normalization) to the maximally mixed state.

### III. RESULTS

Our analysis hinges on mapping the noisy ITE circuit (5) to a noiseless ITE in the doubled Hilbert space, which can be treated efficiently using DMRG. We describe this mapping in detail for single-qubit bit-flip noise before proceeding to consider other noise channels. We focus on the ferromagnetic Ising model with  $J = +1$ , except in our discussion of amplitude damping noise in Sec. III B.

#### A. Pauli noise channels

##### 1. Single-qubit bit-flip noise

We start by considering the ITE in the presence of single-qubit bit-flip errors (also known as  $X$  noise) corresponding to the noise channel

$$\mathcal{N}[\rho] = \prod_i \mathcal{N}_i[\rho], \quad (10)$$

$$\mathcal{N}_i[\rho] = (1-p)\rho + p\sigma_i^x \rho \sigma_i^x, \quad (11)$$

where  $i$  is the qubit index. In the doubled space, this error channel takes the form

$$\tilde{\mathcal{N}} = \prod_i [(1-p) + p\sigma_i^x \otimes \sigma_i^x] = e^{\mu \sum_i (\sigma_i^x \otimes \sigma_i^x - I \otimes I)}, \quad (12)$$

where in the second equality we have used the fact that  $e^{\mu \sum_i \sigma_i^x \otimes \sigma_i^x} = \prod_i e^{\mu \sigma_i^x \otimes \sigma_i^x} = \prod_i [\cosh \mu + \sinh \mu \sigma_i^x \otimes \sigma_i^x]$  and have introduced a parameter  $\mu = \tanh^{-1}[p/(1-p)]$ . This parameter is real and positive for  $0 < p < 1/2$  and in the limit of weak noise,  $p \ll 1$ , becomes  $\mu \sim p + O(p^2)$ . Given Eqs. (7) and (12), in the doubled space the steady

state of the noisy ITE can be written, up to an overall normalization prefactor, as

$$|\rho_{\text{st.s.}}\rangle\rangle \propto \left[ e^{\mu \sum_i (\sigma_i^x \otimes \sigma_i^x)} \prod_m [e^{-\Delta\tau h_m} \otimes (e^{-\Delta\tau h_m})^*] \right]^l |\rho_0\rangle\rangle, \quad (13)$$

where  $l$  is the number of Trotter steps required to reach the steady state. Taking the limit  $\Delta\tau \rightarrow 0$ ,  $\mu \rightarrow 0$  allows one to neglect the Trotter error in the expression (13), which then can be simplified into

$$|\rho_{\text{st.s.}}\rangle\rangle \propto \left[ e^{-\Delta\tau (H \otimes I + I \otimes H^* - \lambda \sum_i \sigma_i^x \otimes \sigma_i^x)} \right]^l |\rho_0\rangle\rangle. \quad (14)$$

Here  $H = \sum_m h_m$  is the Hamiltonian governing the ITE, whereas the newly introduced parameter  $\lambda = \mu/\Delta\tau$  in the case of weak noise describes the error rate per Trotter step,  $\lambda \approx p/\Delta\tau$ . Since noise in state of the art quantum devices can generally be considered weak,  $p \ll 1$  [86–88], hereafter we will refer to  $\lambda$  as an effective error rate.

Equation (14) shows that in the limit  $\Delta\tau, p \rightarrow 0$ ,  $|\rho_{\text{st.s.}}\rangle\rangle$  is the steady state of the ITE with an effective Hamiltonian  $\tilde{H}_{\text{eff}}$  corresponding to two copies of the original system coupled by a noise-induced term  $\tilde{H}_{\mathcal{N}}$ :

$$|\rho_{\text{st.s.}}\rangle\rangle \propto \left[ e^{-\Delta\tau \tilde{H}_{\text{eff}}} \right]^l |\rho_0\rangle\rangle, \quad (15)$$

$$\tilde{H}_{\text{eff}} = H \otimes I + I \otimes H^* + \tilde{H}_{\mathcal{N}}, \quad (16)$$

$$\tilde{H}_{\mathcal{N}} = -\lambda \sum_i \sigma_i^x \otimes \sigma_i^x. \quad (17)$$

Consequently,  $|\rho_{\text{st.s.}}\rangle\rangle$  corresponds to the ground state of  $\tilde{H}_{\text{eff}}$ , and therefore the steady state properties of the noisy ITE, such as the SSB order, can be obtained by studying the ground state of  $\tilde{H}_{\text{eff}}$ .

When the ITE is governed by the transverse-field Ising chain Hamiltonian (3),  $H = H^*$  and  $\tilde{H}_{\text{eff}}$  can be viewed as a transverse-field Ising ladder whose two legs are coupled by a noise-induced  $XX$  term on the rungs. For both the ferromagnetic and the antiferromagnetic model the  $\mathbb{Z}_2$  symmetry generated by  $U = \prod_i \sigma_i^x$  leads to a  $\mathbb{Z}_2 \times \mathbb{Z}_2$  symmetry of the effective Hamiltonian generated by  $U \otimes I$  and  $I \otimes U$ . This  $\mathbb{Z}_2 \times \mathbb{Z}_2$  symmetry corresponds to nothing but the strong (also known as exact) symmetry of the associated noisy evolution [39, 40]. The ground state of the Hamiltonian (16)–(17) thus possesses the  $\mathbb{Z}_2 \times \mathbb{Z}_2$  symmetry as well, unless this symmetry is spontaneously broken. However, it is crucial to emphasize that when this ground state is utilized to calculate the mixed steady state observables via Eq. (9), the  $\mathbb{Z}_2 \times \mathbb{Z}_2$  symmetry breaks down to a global  $\mathbb{Z}_2$  subgroup generated by  $U \otimes U$  due to the overlap with the state  $|I\rangle\rangle$ . This global  $\mathbb{Z}_2$  symmetry corresponds to applying the original  $\mathbb{Z}_2$  symmetry generator to both legs of the ladder simultaneously and represents the weak (or average) symmetry of the noisy evolution. Hence, when observables *linear* in the density matrix are calculated, only the weak symmetry is important and can be spontaneously broken, as the strong symmetry in this case is

broken by default. The situation is different when one is interested in quantities *nonlinear* in the density matrix, such as the Rényi-2 correlator, for which the presence of the strong symmetry is relevant and can lead to various interesting physical phenomena, such as strong-to-weak SSB [49–51, 53, 54].

The SSB of the weak  $\mathbb{Z}_2$  symmetry generated by  $U \otimes U$  leads to the ordered phase in the steady state of the noisy ITE. Since the noise-induced term (17) does not break the weak symmetry (in fact, by itself it even preserves the strong symmetry), we expect the ground state order and phase transition of the Ising chain (3) to persist in the steady state of the noisy ITE, as long as the noise is not too strong and the Trotter error is not too large. Furthermore, since the relevant symmetry of the noisy problem is the same as that of the noiseless one, we expect its universality class to be the same as in the noiseless case (where the transition is in the 2D Ising universality class). The location of the critical point, on the other hand, is nonuniversal and expected to shift in the presence of noise.

To showcase the above statements, we numerically investigate [89] the symmetry breaking order-disorder transition in the steady state of the noisy ITE by computing the ground state of the spin ladder Hamiltonian (16)–(17) using the DMRG [36–38] and then calculating the expectation values of observables in the steady state via Eq. (9). To identify the location of the transition as precisely as possible, we calculate the Binder cumulant [90, 91],

$$U_4 = \frac{1}{2} \left( 3 - \frac{\langle m^4 \rangle}{\langle m^2 \rangle^2} \right), \quad (18)$$

where  $m$  is the order parameter, which for the case of the  $L$ -site ferromagnetic Ising chain is the average magnetization  $m = \sum_i \sigma_i^z / L$ . The Binder cumulant (18) exhibits scale invariance at the critical point  $g = g_c$  [92], whereas near the critical point it is expected to scale with the system size as  $U_4(g, L) = f[(g - g_c)L^{1/\nu}]$ , which allows one to extract the correlation length critical exponent  $\nu$ .

Figure 3(a) depicts the Binder cumulant evaluated for the DMRG-calculated ground state of the spin ladder Hamiltonian (16)–(17) as a function of the transverse field  $g$  for various values of the ladder length  $L$  and open boundary conditions. The Ising couplings along the legs of the ladder are taken to be ferromagnetic, while the strength of the noise-induced couplings along the rungs is set to  $\lambda = 0.1$ . For this value of  $\lambda$  the critical point, identified through the scale invariance of the Binder cumulant, is located at  $g_c \approx 0.94$ , which is slightly lower than the noiseless value of  $g_c = 1$ . The ordered phase is thus still present in the noisy model, although its extent in parameter space is smaller when compared to the noiseless case. The curves representing different system sizes collapse when the Binder cumulant is plotted as a function of  $(g - g_c)L$ , which is illustrated by the inset in Fig. 3(a). The finite size scaling thus yields the correlation length critical exponent of  $\nu = 1$ , which, as expected,



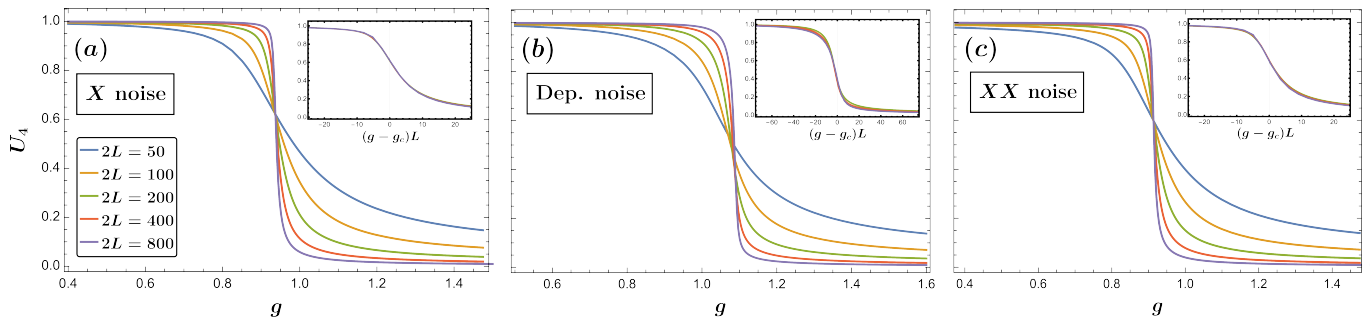


FIG. 3. Binder cumulant from DMRG plotted as a function of the transverse field for the ferromagnetic ( $J = +1$ ) Ising spin ladder (16) with interleg couplings induced by (a) single-qubit bit-flip ( $X$ ) noise given by Eq. (17) with  $\lambda = 0.1$ , (b) single-qubit depolarizing noise given by Eq. (23) with  $\lambda = 0.15$ , and (c) two-qubit bit-flip ( $XX$ ) noise given by Eq. (26) with  $\lambda = 0.1$ . The mixed-state expectation values  $\langle m^2 \rangle$  and  $\langle m^4 \rangle$  entering the expression (18) for the Binder cumulant are computed using Eq. (9). The curves are plotted for various ladder lengths  $L$  in order to identify the scale invariant critical point  $g_c$ ; the total number of sites in each DMRG calculation is equal to  $2L$ . The inset in each subfigure depicts the Binder cumulant as a function of  $(g - g_c)L$  and demonstrates the collapse of the curves corresponding to different system sizes. Open boundary conditions are assumed throughout the DMRG calculations.

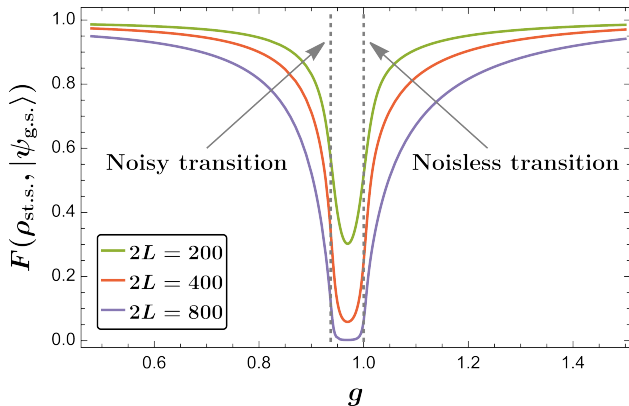


FIG. 4. Fidelity between the mixed noisy steady state  $\rho_{st.s.}$  and the pure target ground state  $|\psi_{g.s.}\rangle$  as a function of the transverse field. The fidelity is computed using the DMRG with open boundary conditions via Eqs. (19)–(20). The noise-induced coupling in the effective Hamiltonian is set to  $\lambda = 0.1$ . The dotted lines indicate the critical points for the SSB transition in the noisy ( $g_c \approx 0.94$ ) and noiseless ( $g_c = 1$ ) steady state. A small symmetry-breaking field is added at the ends of the spin ladder to ensure that the DMRG algorithm finds a symmetry-broken ground state within the ground-state manifold.

belongs to the 2D Ising universality class.

In addition to identifying the presence of the SSB order in the noisy steady state  $\rho_{st.s.}$ , we also quantify how “close” this state is to the target state, namely the ground state  $|\psi_{g.s.}\rangle$  of the original Hamiltonian  $H$ . We quantify this with the fidelity,

$$F(\rho_{st.s.}, |\psi_{g.s.}\rangle) = \langle \psi_{g.s.} | \rho_{st.s.} | \psi_{g.s.} \rangle = \text{Tr}[\rho_{st.s.} \rho_{g.s.}], \quad (19)$$

where  $\rho_{g.s.} = |\psi_{g.s.}\rangle\langle\psi_{g.s.}|$  is the pure state density matrix corresponding to the ground state of  $H$ . Within the doubled space formalism, the trace in Eq. (19) can be

evaluated as an overlap between the ground states of the effective Hamiltonian with and without the noise-induced coupling:

$$\text{Tr}[\rho_{st.s.} \rho_{g.s.}] = \langle\langle \rho_{g.s.} | \rho_{st.s.} \rangle\rangle. \quad (20)$$

We compute the two ground states, one with  $\lambda = 0.1$  and the other with  $\lambda = 0$ , and the overlap between them using DMRG, and plot the resulting fidelity as a function of the transverse field in Fig. 4. For  $g \ll 1$  ( $g \gg 1$ ), both the noisy and the noiseless steady state are deep in their respective ordered (disordered) phases, and the fidelity between them is close to one. On the other hand, for values of  $g$  in between the noiseless and the noisy critical points (marked by dotted lines in the figure), the noisy steady state is disordered, while the noiseless one is ordered, and the fidelity dips drastically toward zero. The dip is stronger for larger system sizes, with the fidelity reaching zero for  $2L = 800$ . We note that the fidelity also decreases with system size even deep in the ordered/disordered phase, albeit the decrease is much smaller there than in the region between the critical points.

Using the DMRG, we further calculate the location of the critical point  $g_c$  for other values of the parameter  $\lambda$  and plot the resulting two-dimensional phase diagram in the  $(g, \lambda)$  parameter space in Fig. 5(a). This phase diagram demonstrates that in the limit  $\Delta\tau, p \rightarrow 0$  of the noisy ITE the ordered phase is stable in the presence of the single-qubit bit-flip noise, and survives as long as the effective error rate  $\lambda = p/\Delta\tau$  is below the upper critical value of  $\lambda_{c,\max} \approx 2$ . This calculation therefore validates the schematic picture shown in Fig. 1.

While we have numerically shown the stability of the ordered phase against the  $X$  noise in the limit where both the Trotter step and the noise strength are small ( $\Delta\tau, p \rightarrow 0$ ) such that the effective Hamiltonian picture (16)–(17) applies, an actual implementation of the

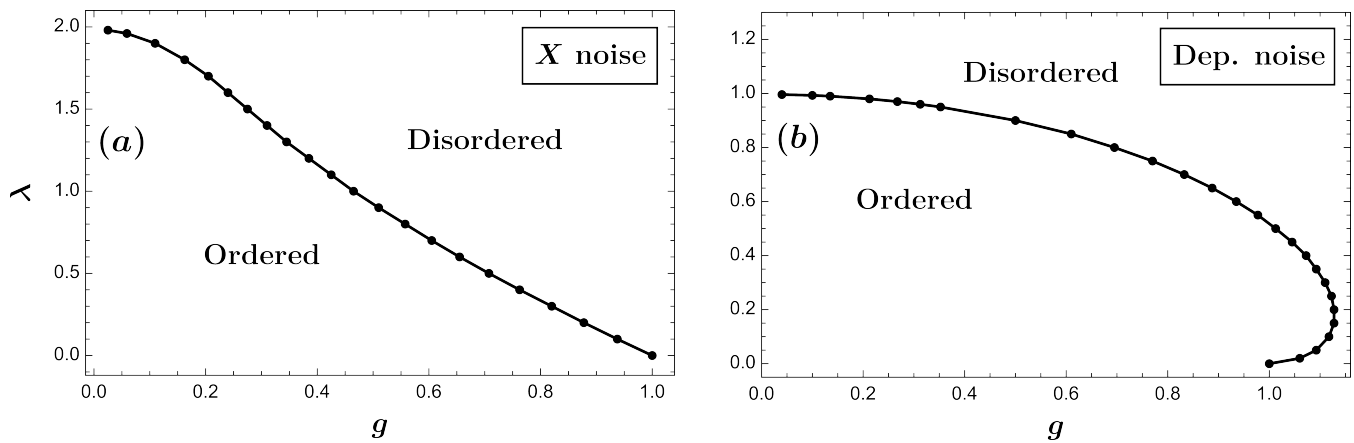


FIG. 5. Phase diagram for the ferromagnetic ( $J = +1$ ) Ising spin ladder model (16) when the interleg couplings are induced by (a) single-qubit bit-flip ( $X$ ) noise given by Eq. (17) and (b) single-qubit depolarizing noise given by Eq. (23). The phase boundaries are obtained by computing the Binder cumulant (18) using the DMRG and extracting the scale-invariant crossings between (a) the  $2L = 200$  and  $2L = 400$  curves and (b) the  $2L = 400$  and  $2L = 800$  curves.

ITE on quantum hardware would have a finite Trotter step and a finite noise strength. To investigate whether the SSB ordered phase and the phase transition are still present in that latter scenario, we numerically simulate [89] the density matrix throughout the noisy ITE process for small system sizes on a classical high-performance computer with graphics processing units (GPUs). The simulated circuit is schematically depicted in Fig. 2(a).

The results of these density matrix simulations are represented by solid curves in Fig. 6(a), which, similarly to Fig. 3(a), depicts the Binder cumulant as a function of the transverse field for various lengths of the chain. The Binder cumulant in this case is calculated for the steady state of the noisy ITE process with a finite Trotter step  $\Delta\tau = 0.1$  and the effective error rate of  $\lambda = p/\Delta\tau = 0.1$ . When simulating the noisy ITE, we take ferromagnetically fully ordered state  $|\uparrow\uparrow\dots\uparrow\rangle$  as the initial state, but we checked that starting with an antiferromagnetically ordered or a disordered state yields the same results. The dashed curves in Fig. 6(a) on the other hand represent the Binder cumulant calculated from DMRG on the effective Hamiltonian (16)–(17), and thus represent the limit  $\Delta\tau, p \rightarrow 0$  of the noisy ITE with the same  $\lambda = p/\Delta\tau = 0.1$  [93]. The scale invariant crossing of the solid curves in Fig. 6(a) illustrates that the ordered phase and the phase transition are present in the noisy ITE even if  $\Delta\tau$  is finite. Still, finite Trotter error slightly shifts the curves and the scale invariant point from the results in the limit  $\Delta\tau, p \rightarrow 0$ . This shift can be systematically reduced by reducing the Trotter step size. We demonstrate this by plotting the Binder cumulant versus transverse field curves for various values of the Trotter step, ranging from  $\Delta\tau = 0.01$  to  $\Delta\tau = 0.1$ , together with the  $\Delta\tau \rightarrow 0$  results, in Fig. 6(b). Here we fix the effective error rate to  $\lambda = p/\Delta\tau = 0.1$  and the chain length to  $L = 13$  sites. These results validate the reliability of the

effective Hamiltonian approach in the limit of weak noise. Given the advantages of the DMRG approach in terms of scalability and mitigating finite-size effects, we therefore restrict our focus to this approach for the remainder of the paper.

## 2. Single-qubit depolarizing noise

Next, we study ITE in the presence of the single-qubit depolarizing noise. This noise channel reads:

$$\mathcal{N}[\rho] = \prod_i \mathcal{N}_i[\rho], \quad (21)$$

$$\mathcal{N}_i[\rho] = (1-p)\rho + \frac{p}{3}\sigma_i^x\rho\sigma_i^x + \frac{p}{3}\sigma_i^y\rho\sigma_i^y + \frac{p}{3}\sigma_i^z\rho\sigma_i^z, \quad (22)$$

where  $i$  is again the qubit index. For the depolarizing noise one can also derive an effective Hamiltonian in the doubled Hilbert space, the ground state of which describes the mixed steady state of the noisy ITE in the  $\Delta\tau, p \rightarrow 0$  limit. This effective Hamiltonian also takes the form of a spin ladder, see Eq. (16), but with a different noise-induced coupling on the rungs:

$$\tilde{H}_{\mathcal{N}} = -\frac{\lambda}{3} \sum_i (\sigma_i^x \otimes \sigma_i^x - \sigma_i^y \otimes \sigma_i^y + \sigma_i^z \otimes \sigma_i^z), \quad (23)$$

where the minus sign in the  $\sigma_i^y \otimes \sigma_i^y$  term is present due to the complex conjugation appearing in Eq. (8). Here we have introduced  $\lambda = \mu/\Delta\tau$  and  $\mu = -3/4 \log(1 - 4p/3)$ ; the parameter  $\mu$  is real and positive for  $0 < p < 3/4$ . Akin to the case of the bit-flip error, here the weak noise limit yields  $\mu \sim p + O(p^2)$  and thus in this limit the parameter  $\lambda$  describes the effective error rate per the ITE Trotter step,  $\lambda \approx p/\Delta\tau$ .

In the ferromagnetic case, the Hamiltonian (23) breaks the strong  $\mathbb{Z}_2 \times \mathbb{Z}_2$  symmetry, but preserves the weak  $\mathbb{Z}_2$

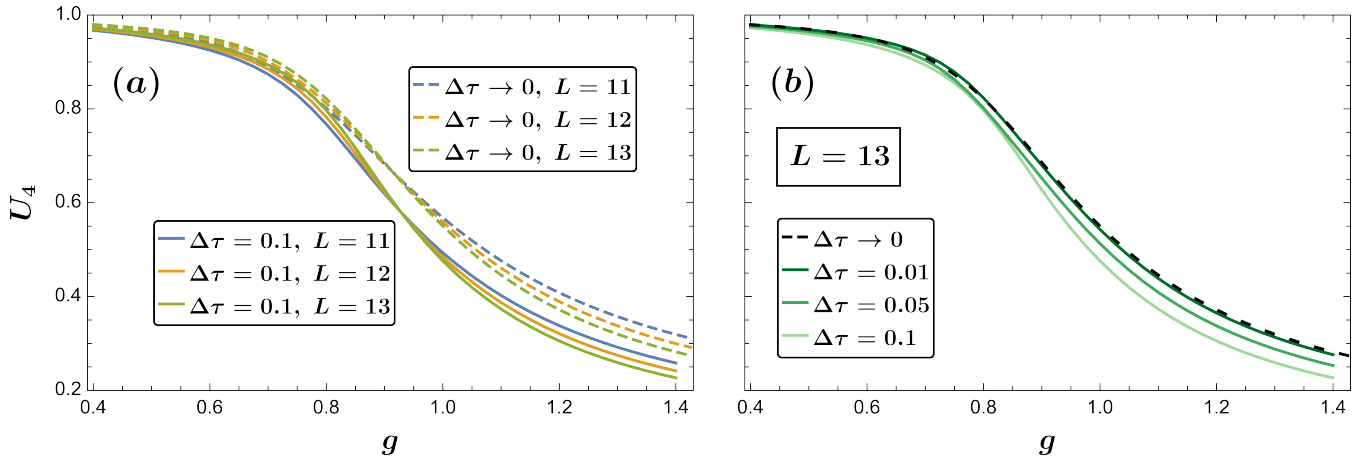


FIG. 6. (a) Solid lines: Binder cumulant plotted as a function of the transverse field for the steady state of a directly simulated density matrix throughout the noisy ITE process with ferromagnetic couplings ( $J = +1$ ),  $X$  noise and a finite ( $\Delta\tau = 0.1$ ) Trotter step. Ferromagnetically fully ordered state is taken as the initial state for the noisy ITE simulations. Dashed lines: same curves but plotted for the DMRG-calculated ground state of the Ising spin ladder model (16) with the  $X$ -noise-induced interleg couplings (17). The dashed lines represent the results for the noisy ITE with a vanishing Trotter step ( $\Delta\tau \rightarrow 0$ ). In both cases the curves are plotted for various spin chain/ladder lengths  $L$  in order to identify the scale invariant point. The effective error rate in both cases is set to  $\lambda = 0.1$  and open boundary conditions are assumed. (b) Same curves but plotted for a fixed length of the spin chain/ladder ( $L = 13$ ) and various values of the ITE Trotter step.

symmetry generated by the simultaneous bit-flip on both chains, which is the relevant symmetry when calculating the mixed steady-state observables linear in the density matrix. Hence, we expect the SSB order and the phase transition in the steady state of the ITE to be stable in the presence of the depolarizing noise, and we further expect the noisy transition to belong to the same 2D Ising universality class.

To numerically confirm these expectations, similarly to the  $X$ -noise spin ladder (16)–(17), here we calculate the ground state of the depolarizing-noise spin ladder (16),(23) with DMRG and plot the Binder cumulant extracted for that ground state as a function of the transverse field for various system sizes in Fig. 3(b). The interleg coupling is set to  $\lambda = 0.15$ . As depicted in Fig. 3(b), for this value of  $\lambda$  the almost-scale-invariant crossing point of curves for different system sizes is shifted from a noiseless value of  $g = 1$  to a value  $g > 1$ , in contrast to the model with  $X$  noise where the shift was toward a value of  $g < 1$ . The “almost” scale invariance of the crossing and its size-dependent drift can be explained by the presence of finite-size corrections to the Binder cumulant near the critical point. In this work, the maximum system size that we numerically analyze is  $2L = 800$ , and the crossing between the  $2L = 800$  and  $2L = 400$  curves for  $\lambda = 0.15$  occurs at  $g_c \approx 1.09$ . However, the finite-size drift suggests that the actual critical point is located at a slightly larger value of  $g$ . Notably, this drift appears stronger for the depolarizing noise model than for the bit-flip noise model; this can be seen by examining the inset of Fig. 3(b), which depicts the Binder cumulant as a function of  $(g - g_c)L$ . While the inset curves do collapse close to each other, suggesting the same correlation

length critical exponent of  $\nu = 1$  as in the case of the bit-flip noise, the collapse is not as dense as the one depicted in the inset of Fig. 3(a).

By calculating the crossing points between the  $2L = 400$  and  $2L = 800$  curves for various values of  $\lambda$ , we obtain an approximate phase diagram in the  $(g, \lambda)$  plane for the steady state of the noisy ITE with the depolarizing noise in the  $\Delta\tau, p \rightarrow 0$  limit. This phase diagram is plotted in Fig. 5(b). We emphasize that the computed phase boundary is approximate due to the aforementioned finite-size drift of the crossing, but we expect the true phase boundary to lie close to the one we obtained.

In contrast to the phase diagram for the bit-flip noise in Fig. 5(a), here the critical  $g_c$ , and with it the extent of the ordered phase, first increases as  $\lambda$  is raised. Past a certain value of  $\lambda$ , which appears to be close to  $\lambda = 0.2$ , the critical value of  $g_c$  starts to decrease. Consequently, and perhaps contrary to naive expectations, the maximal extent of the ordered phase in the  $g$  parameter space is reached at a nonzero level of noise. We speculate that this phenomenon can be attributed to the fact that  $\sigma_i^z$  operators within the depolarizing noise channel anticommute with  $\sigma_i^x$  operators within the  $e^{-\Delta\tau g \sigma_i^x}$  part of an ITE step, which may, for a small level of noise and after averaging over different quantum trajectories, effectively reduce the value of the transverse field felt by the system, thus requiring larger values of  $g$  to move out of the ordered phase. Overall, Fig. 5(b) illustrates that similarly to the case of  $X$  noise, the ITE in the presence of the single-qubit depolarizing noise boasts a stable SSB ordered phase, and the order survives up to a maximum effective error rate of  $\lambda_{c,\max} \approx 1$ . This example also

highlights that it is the weak  $\mathbb{Z}_2$  rather than the strong  $\mathbb{Z}_2 \times \mathbb{Z}_2$  symmetry that protects the SSB transition in the noisy ITE.

### 3. Two-qubit bit-flip noise

We now investigate ITE in the presence of a two-qubit noise. As a particular example, we take the two-qubit bit-flip ( $XX$ ) noise, the error channel for which can be written as

$$\mathcal{N}[\rho] = \prod_i \mathcal{N}_{i,i+1}[\rho], \quad (24)$$

$$\mathcal{N}_{i,i+1}[\rho] = (1-p)\rho + p\sigma_i^x \sigma_{i+1}^x \rho \sigma_i^x \sigma_{i+1}^x, \quad (25)$$

where  $i$  is the qubit index. This noise channel induces correlated errors, whereby a bit flip on site  $i$  is always accompanied by a bit flip on site  $i+1$ . The effective Hamiltonian in the doubled Hilbert space in this case can be obtained in exactly the same fashion as the one for the ITE with the single-qubit bit-flip noise. The effective Hamiltonian is again an Ising spin ladder, but with plaquette-type interleg coupling:

$$\tilde{H}_{\mathcal{N}} = -\lambda \sum_i \sigma_i^x \sigma_{i+1}^x \otimes \sigma_i^x \sigma_{i+1}^x. \quad (26)$$

Here, as before,  $\lambda = \mu/\Delta\tau$ ,  $\mu = \tanh^{-1}[p/(1-p)]$ , and in the weak noise limit  $\lambda \approx p/\Delta\tau$  represents the effective error rate. Note that in the ferromagnetic case the Hamiltonian (26) preserves the weak  $\mathbb{Z}_2$  symmetry generated by the simultaneous bit-flip on both legs of the ladder. Therefore, similarly to the single-qubit noise types considered before, here we expect the SSB order and associated transition to be stable and to remain within the 2D Ising universality class.

The Binder cumulant computed from DMRG on the effective Hamiltonian (16),(26) with interleg coupling  $\lambda = 0.1$  is shown in Fig. 3(c). Overall, the behavior of the Binder cumulant in this case is very similar to the one presented for the case of the single-qubit bit-flip noise in the beginning of this section. The scale-invariant crossing of the curves corresponding to different lengths of the spin ladder is located at  $g_c \approx 0.91$ , indicating the presence of the critical point and the SSB phase transition. The Binder cumulant, plotted as a function of  $(g - g_c)L$  in the inset of the figure, shows the collapse of the curves corresponding to different system sizes and suggests a correlation length critical exponent of  $\nu = 1$ . Note that for this type of noise the finite-size drift of the crossing is more akin to the (very slight) drift occurring in the case of the  $X$ -noise and is not as strong as that observed for the case of the depolarizing noise. We opt out of presenting the full phase diagram in the  $(g, \lambda)$  plane for this type of noise since it very closely resembles the already computed phase diagram for the single-qubit bit-flip noise, see Fig. 5(a), indicating that the SSB ordered phase is stable under the noisy ITE even in the

presence of correlated two-qubit noise, such as the  $XX$  noise considered here.

In fact, we expect the phase transition to persist in the presence of *any* Pauli noise. For any such noise, the interleg coupling in the effective Hamiltonian is of the form

$$\tilde{H}_{\mathcal{N}} = \sum_m c_m P_m \otimes P_m^*, \quad (27)$$

where  $\{P_m\}$  are a set of Pauli strings and  $c_m$  are real coefficients that depend on the noise strength. Since any Pauli string  $P_m$  either commutes or anticommutes with the  $\mathbb{Z}_2$  symmetry generator  $U = \prod_i \sigma_i^x$ , the weak symmetry generator  $U \otimes U$  always commutes with  $P_m \otimes P_m^*$ .

### B. Amplitude damping noise channel

We now move beyond Pauli noise by considering ITE under the amplitude damping (AD) noise channel. The amplitude damping is an example of a non-unital quantum channel. It models energy dissipation effects in open quantum systems [2]. In terms of Kraus operators, this channel can be written as

$$\mathcal{N}[\rho] = \prod_i \mathcal{N}_i[\rho], \quad (28)$$

$$\mathcal{N}_i[\rho] = K_{0,i} \rho K_{0,i}^\dagger + K_{1,i} \rho K_{1,i}^\dagger, \quad (29)$$

where

$$K_{0,i} = \frac{1 + \sqrt{1-p}}{2} + \frac{1 - \sqrt{1-p}}{2} \sigma_i^z, \quad (30)$$

$$K_{1,i} = \sqrt{p} \sigma_i^+. \quad (31)$$

The effective Hamiltonian in the doubled space now corresponds to an Ising spin ladder with the following noise-induced term:

$$\tilde{H}_{\mathcal{N}} = -\frac{\lambda_z}{4} \sum_i (\sigma_i^z \otimes I + I \otimes \sigma_i^z) - \lambda_+ \sum_i \sigma_i^+ \otimes \sigma_i^+, \quad (32)$$

where  $\sigma_i^+ = (\sigma_i^x + i\sigma_i^y)/2$  and we have introduced parameters  $\lambda_{z,+} = \mu_{z,+}/\Delta\tau$  and  $\mu_z = -\log(1-p)$ ,  $\mu_+ = p$ . The limit of weak noise,  $p \ll 1$ , gives  $\mu_z \approx p + O(p^2)$  and in this case both  $\lambda_z$  and  $\lambda_+$  represent the effective noise rate,  $\lambda_{z,+} \approx p/\Delta\tau$ . The first sum in the Hamiltonian (32) represents a longitudinal field added to each leg of the Ising spin ladder, while the second sum is a non-Hermitian coupling along the rungs. The entire effective Hamiltonian (16),(32) is thus non-Hermitian; however, being completely real it possesses a  $\mathcal{PT}$  symmetry [94–96] and its eigenvalues are either real or come in complex-conjugated pairs.

If the Ising ladder has ferromagnetic couplings along its legs, the Hamiltonian (32), in addition to breaking the strong  $\mathbb{Z}_2 \times \mathbb{Z}_2$  symmetry, also breaks the weak  $\mathbb{Z}_2$  symmetry generated by the simultaneous bit-flip on both legs of



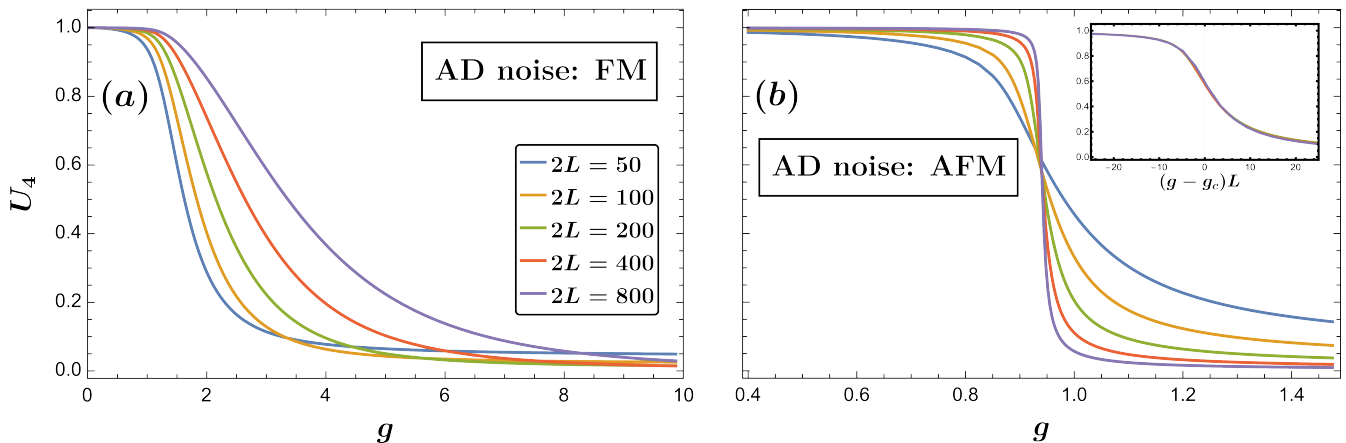


FIG. 7. Binder cumulant plotted as a function of the transverse field and calculated using the DMRG for (a) the ferromagnetic (FM,  $J = +1$ ) and (b) the antiferromagnetic (AFM,  $J = -1$ ) Ising spin ladder model (16) when the interleg coupling is induced by the amplitude damping (AD) noise given by Eq. (32) with  $\lambda_z = \lambda_+ = 0.4$ . The curves are plotted for various ladder lengths  $L$  in order to identify the absence (in the FM case) or the presence (in the AFM case) of the scale invariant critical point  $g_c$ ; the total number of sites in the DMRG calculation is equal to  $2L$ . The inset in (b) depicts the Binder cumulant as a function of  $(g - g_c)L$  and demonstrates the collapse of the curves corresponding to different system sizes. Open boundary conditions are assumed throughout the calculations in both (a) and (b).

the ladder. Consequently, the ground state of the combined Hamiltonian (16),(32) is not expected to exhibit SSB. We confirm this by calculating the Binder cumulant as a function of the transverse field using DMRG for various lengths of the spin ladder, see Fig. 7(a). Note that the DMRG calculation here is done for a non-Hermitian Hamiltonian and yet yields a real ground state energy and observables, thus manifesting the aforementioned  $\mathcal{PT}$  symmetry. As opposed to the  $U_4$  versus  $g$  plots presented earlier (see Fig. 3), here the curves corresponding to different system sizes intersect at different  $g$  values, demonstrating the absence of a scale invariant crossing, and, hence, the phase transition. This behavior of the Binder cumulant closely resembles the one occurring in the ferromagnetic mixed-field Ising chain, where it is well-known that the Ising symmetry and the SSB order are absent. Given these results, we conclude that the SSB ordered phase and phase transition present in the steady state of noiseless ITE under the ferromagnetic quantum Ising Hamiltonian does not survive when the ITE is subject to AD noise.

The situation is drastically different for the antiferromagnetic Ising chain. The order parameter in this case is the staggered magnetization  $m_s = \sum_i (-1)^i \sigma_i^z / L$ , which, when finite, indicates a breaking of both global spin-flip and mirror reflection symmetries. In this case, explicitly breaking the global spin-flip symmetry by adding a uniform longitudinal field  $h$  leaves the residual mirror symmetry intact, leading to a nontrivial phase diagram in the  $(g, h)$  plane for the antiferromagnetic mixed-field Ising model [97]. In the doubled space, the AD-noise-induced Hamiltonian (32) also preserves the relevant weak  $\mathbb{Z}_2$  symmetry, which in this case is the mirror symmetry with respect to the plane perpendicular to the

ladder, and thus the model (16),(32) should exhibit the SSB order and the phase transition. This is demonstrated in Fig. 7(b), where as before we depict the Binder cumulant as a function of the transverse field for various ladder lengths and set  $J = -1$ . This figure is similar to those presented for the other types of noise to which the transition is robust, see Fig. 3. The Binder cumulant displays a scale-invariant crossing at  $g_c \approx 0.94$ . The inset displays the collapse of the curves as a function of  $(g - g_c)L$  and indicates the expected critical exponent of  $\nu = 1$ . These results further corroborate our main conclusion that the SSB ordered phase in the steady state of the noisy ITE is stable against noise as long as the noise preserves the underlying weak symmetry of the evolution.

#### IV. CONCLUSION

In this paper we studied whether ITE-based preparation of SSB ground state order on a quantum computer is robust to noise. For the sake of generality and simplicity, we did not consider any particular ITE algorithm, instead focusing on a black box approach representing ITE as a Trotterized imaginary-time “circuit” and investigating the SSB in the mixed steady state of that circuit. The main conclusion of our work is that, given a target Hamiltonian with a ground state that spontaneously breaks a symmetry, the preparation of the ground state order using the ITE is robust against noise, as long as the noise channel respects the weak version of that symmetry. The strong version of the symmetry, on the other hand, does not play a role in the preparation of the SSB order, since all the relevant observables are linear in the density operator.

To illustrate these conclusions, we employed the Choi-Jamiołkowski isomorphism and in the limit of weak noise and small imaginary-time Trotter step mapped the noisy ITE to a noiseless ITE under an effective Hamiltonian in the doubled Hilbert space. This effective Hamiltonian, in general, corresponds to two copies of the original target Hamiltonian coupled by noise-induced terms, and in the one-dimensional case its ground state can be efficiently computed using the DMRG. Focusing on a concrete example of the one-dimensional transverse-field Ising model as a target Hamiltonian and various types of noise affecting the ITE, we employed DMRG to compute the ground state of the effective Hamiltonian, which in this case corresponds to an Ising spin ladder, and applied the obtained results to study the SSB order and the associated phase transition in the mixed steady state of the noisy ITE. In addition, for comparatively small system sizes we directly simulated the evolution of the density matrix under the noisy ITE to show that our conclusions hold in the case of a small but finite Trotter step.

We conclude by discussing implications of our work for practical simulations of the ITE on noisy quantum devices. While in this work we modeled the ITE as a black box, an algorithm implementing the ITE, which is a non-unitary protocol, on a device [11–28] requires the introduction of certain nontrivial operations, such as mid-circuit measurements and feedback [28]. Still, we generally expect our results to hold for a realistic protocol implementing the ITE as long as at each step the (noiseless) protocol well approximates an ITE step, and the state is moved closer to the target ground state. However, not all protocols implement the ITE in that fashion, and it would be interesting to “open up” the ITE black box and investigate the robustness of phase preparation against noise in various specific ITE quantum algorithms.

Another potential future direction is to study how the Trotter error affects the preparation of the ground state order, and whether a phenomenon like the Trotter-error-induced phase transition [98] can occur within this model.

Another interesting direction to explore within this context is the use of noise tailoring techniques like Pauli twirling [99, 100] and probabilistic error cancellation/reduction [101–103]. In this approach, the target circuit implementing, e.g., noisy ITE is replaced by a (quasi)probabilistic ensemble of circuits over which observable calculations are averaged. Up to finite sampling error and possible signal-to-noise issues, the result is an effective circuit with a modified noise. For example, Pauli twirling of Clifford gates can convert a generic noise channel into a Pauli noise channel [99]. This is potentially valuable in cases, like that of the ferromagnetic order in the Ising chain considered here, where it is desirable for the noise to take a Pauli form. The possible extension of our results to specific implementations of ITE quantum algorithms in concert with such noise tailoring and error mitigation techniques thus offers the intriguing prospect of a noise-resilient approach to quantum state preparation.

#### ACKNOWLEDGMENTS

We thank Peter Orth, Haining Pan, Jedediah Pixley, and Justin Wilson for fruitful discussions. This work was supported by the U.S. Department of Energy, Office of Science, Basic Energy Sciences, Materials Science and Engineering Division, including the grant of computer time at the National Energy Research Scientific Computing Center (NERSC) in Berkeley, California. This part of research was performed at the Ames National Laboratory, which is operated for the U.S. DOE by Iowa State University under Contract No. DE-AC02-07CH11358.

- 
- [1] A. Y. Kitaev, [arXiv:quant-ph/9511026](https://arxiv.org/abs/quant-ph/9511026) (1995), [10.48550/arXiv.quant-ph/9511026](https://arxiv.org/abs/10.48550/arXiv.quant-ph/9511026).
  - [2] M. A. Nielsen and I. L. Chuang, *Quantum Computation and Quantum Information: 10th Anniversary Edition*, 10th ed. (Cambridge University Press, New York, USA, 2011).
  - [3] B. Bauer, S. Bravyi, M. Motta, and G. K.-L. Chan, *Chem. Rev.* **120**, 12685 (2020).
  - [4] A. M. Dalzell, S. McArdle, M. Berta, P. Bienias, C.-F. Chen, A. Gilyén, C. T. Hann, M. J. Kastoryano, E. T. Khabiboulline, A. Kubica, G. Salton, S. Wang, and F. G. S. L. Brandão, “Quantum algorithms: A survey of applications and end-to-end complexities,” (2023), [arXiv:2310.03011](https://arxiv.org/abs/2310.03011) [quant-ph].
  - [5] E. Farhi, J. Goldstone, S. Gutmann, and M. Sipser, “Quantum computation by adiabatic evolution,” (2000), [arXiv:quant-ph/0001106](https://arxiv.org/abs/quant-ph/0001106) [quant-ph].
  - [6] E. Farhi, J. Goldstone, S. Gutmann, J. Lapan, A. Lundgren, and D. Preda, *Science* **292**, 472 (2001).
  - [7] T. Albash and D. A. Lidar, *Rev. Mod. Phys.* **90**, 015002 (2018).
  - [8] A. Peruzzo, J. McClean, P. Shadbolt, M.-H. Yung, X.-Q. Zhou, P. J. Love, A. Aspuru-Guzik, and J. L. O’Brien, *Nat. Commun.* **5**, 1 (2014).
  - [9] J. R. McClean, J. Romero, R. Babbush, and A. Aspuru-Guzik, *New J. Phys.* **18**, 023023 (2016).
  - [10] J. Romero, R. Babbush, J. R. McClean, C. Hempel, P. J. Love, and A. Aspuru-Guzik, *Quantum Sci. Technol.* **4**, 014008 (2018).
  - [11] M. Motta, C. Sun, A. T. Tan, M. J. O’Rourke, E. Ye, A. J. Minnich, F. G. Brandão, and G. K.-L. Chan, *Nat. Phys.* **16**, 205 (2020).
  - [12] S.-N. Sun, M. Motta, R. N. Tazhigulov, A. T. Tan, G. K. Chan, and A. J. Minnich, [arXiv:2009.03542](https://arxiv.org/abs/2009.03542) (2020).
  - [13] K. Yeter-Aydeniz, R. C. Pooser, and G. Siopsis, *npj Quantum Inf.* **6**, 1 (2020).
  - [14] H. Nishi, T. Kosugi, and Y.-i. Matsushita, *npj Quantum Inf.* **7**, 85 (2021).
  - [15] H. Kamakari, S.-N. Sun, M. Motta, and A. J. Minnich, *PRX Quantum* **3**, 010320 (2022).
  - [16] K. Yeter-Aydeniz, E. Moschandreou, and G. Siopsis, *Phys. Rev. A* **105**, 012412 (2022).

- [17] K. Hejazi, M. Motta, and G. K.-L. Chan, “Adiabatic quantum imaginary time evolution,” (2024), [arXiv:2308.03292 \[quant-ph\]](#).
- [18] S. McArdle, T. Jones, S. Endo, Y. Li, S. C. Benjamin, and X. Yuan, [npj Quantum Inf.](#) **5**, 75 (2019).
- [19] T. Jones, S. Endo, S. McArdle, X. Yuan, and S. C. Benjamin, [Phys. Rev. A](#) **99**, 062304 (2019).
- [20] S. Endo, J. Sun, Y. Li, S. C. Benjamin, and X. Yuan, [Phys. Rev. Lett.](#) **125**, 010501 (2020).
- [21] X. Yuan, S. Endo, Q. Zhao, Y. Li, and S. C. Benjamin, [Quantum](#) **3**, 191 (2019).
- [22] N. Gomes, A. Mukherjee, F. Zhang, T. Iadecola, C.-Z. Wang, K.-M. Ho, P. P. Orth, and Y.-X. Yao, [Adv. Quantum Technol.](#) **4**, 2100114 (2021).
- [23] N. Gomes, F. Zhang, N. F. Berthussen, C.-Z. Wang, K.-M. Ho, P. P. Orth, and Y.-X. Yao, [J. Chem. Theory Comput.](#) **16**, 6256 (2020).
- [24] H. Chen, N. Gomes, S. Niu, and W. A. d. Jong, [Quantum](#) **8**, 1252 (2024).
- [25] T. Liu, J.-G. Liu, and H. Fan, [Quantum Information Processing](#) **20**, 204 (2021).
- [26] S.-H. Lin, R. Dilip, A. G. Green, A. Smith, and F. Pollmann, [PRX Quantum](#) **2**, 010342 (2021).
- [27] T. Kosugi, Y. Nishiya, H. Nishi, and Y.-i. Matsushita, [Phys. Rev. Res.](#) **4**, 033121 (2022).
- [28] Y. Mao, M. Chaudhary, M. Kondappan, J. Shi, E. O. Ilo-Okeke, V. Ivannikov, and T. Byrnes, [Phys. Rev. Lett.](#) **131**, 110602 (2023).
- [29] J. M. Koh, S.-N. Sun, M. Motta, and A. J. Minnich, [Nature Physics](#) **19**, 1314 (2023).
- [30] M. Iqbal, N. Tantivasadakarn, T. M. Gatterman, J. A. Gerber, K. Gilmore, D. Gresh, A. Hankin, N. Hewitt, C. V. Horst, M. Matheny, T. Mengle, B. Neyenhuis, A. Vishwanath, M. Foss-Feig, R. Verresen, and H. Dreyer, “Topological order from measurements and feed-forward on a trapped ion quantum computer,” (2023), [arXiv:2302.01917 \[quant-ph\]](#).
- [31] M. Foss-Feig, A. Tikku, T.-C. Lu, K. Mayer, M. Iqbal, T. M. Gatterman, J. A. Gerber, K. Gilmore, D. Gresh, A. Hankin, N. Hewitt, C. V. Horst, M. Matheny, T. Mengle, B. Neyenhuis, H. Dreyer, D. Hayes, T. H. Hsieh, and I. H. Kim, “Experimental demonstration of the advantage of adaptive quantum circuits,” (2023), [arXiv:2302.03029 \[quant-ph\]](#).
- [32] J. Preskill, [Lecture Notes for Physics 229:Quantum Information and Computation](#) (CreateSpace Independent Publishing Platform, 2015).
- [33] This Trotterized approach to ITE is also implemented directly in a variety of classical algorithms for quantum many-body physics, including time-evolving block decimation [104, 105] and various quantum Monte Carlo approaches [106–109].
- [34] A. Jamiolkowski, [Reports on Mathematical Physics](#) **3**, 275 (1972).
- [35] M.-D. Choi, [Linear Algebra and its Applications](#) **10**, 285 (1975).
- [36] S. R. White, [Phys. Rev. Lett.](#) **69**, 2863 (1992).
- [37] S. R. White, [Phys. Rev. B](#) **48**, 10345 (1993).
- [38] U. Schollwöck, [Rev. Mod. Phys.](#) **77**, 259 (2005).
- [39] B. Buča and T. Prosen, [New Journal of Physics](#) **14**, 073007 (2012).
- [40] C. de Groot, A. Turzillo, and N. Schuch, [Quantum](#) **6**, 856 (2022).
- [41] M. F. Maghrebi and A. V. Gorshkov, [Phys. Rev. B](#) **93**, 014307 (2016).
- [42] V. R. Overbeck, M. F. Maghrebi, A. V. Gorshkov, and H. Weimer, [Phys. Rev. A](#) **95**, 042133 (2017).
- [43] J. Jin, A. Biella, O. Viyuela, C. Ciuti, R. Fazio, and D. Rossini, [Phys. Rev. B](#) **98**, 241108 (2018).
- [44] S. Lieu, R. Belyansky, J. T. Young, R. Lundgren, V. V. Albert, and A. V. Gorshkov, [Phys. Rev. Lett.](#) **125**, 240405 (2020).
- [45] A. Coser and D. Pérez-García, [Quantum](#) **3**, 174 (2019).
- [46] R. Ma and C. Wang, [Phys. Rev. X](#) **13**, 031016 (2023).
- [47] J. Y. Lee, Y.-Z. You, and C. Xu, “Symmetry protected topological phases under decoherence,” (2024), [arXiv:2210.16323 \[cond-mat.str-el\]](#).
- [48] J.-H. Zhang, Y. Qi, and Z. Bi, “Strange correlation function for average symmetry-protected topological phases,” (2024), [arXiv:2210.17485 \[cond-mat.str-el\]](#).
- [49] R. Ma, J.-H. Zhang, Z. Bi, M. Cheng, and C. Wang, “Topological phases with average symmetries: the decohered, the disordered, and the intrinsic,” (2024), [arXiv:2305.16399 \[cond-mat.str-el\]](#).
- [50] L. A. Lessa, R. Ma, J.-H. Zhang, Z. Bi, M. Cheng, and C. Wang, “Strong-to-weak spontaneous symmetry breaking in mixed quantum states,” (2024), [arXiv:2405.03639 \[quant-ph\]](#).
- [51] J. Y. Lee, C.-M. Jian, and C. Xu, [PRX Quantum](#) **4**, 030317 (2023).
- [52] Y. Bao, R. Fan, A. Vishwanath, and E. Altman, “Mixed-state topological order and the errorfield double formulation of decoherence-induced transitions,” (2023), [arXiv:2301.05687 \[quant-ph\]](#).
- [53] R. Ma and A. Turzillo, “Symmetry protected topological phases of mixed states in the doubled space,” (2024), [arXiv:2403.13280 \[quant-ph\]](#).
- [54] P. Sala, S. Gopalakrishnan, M. Oshikawa, and Y. You, “Spontaneous strong symmetry breaking in open systems: Purification perspective,” (2024), [arXiv:2405.02402 \[quant-ph\]](#).
- [55] S. Sang, Y. Zou, and T. H. Hsieh, “Mixed-state quantum phases: Renormalization and quantum error correction,” (2023), [arXiv:2310.08639 \[quant-ph\]](#).
- [56] T. Rakovszky, S. Gopalakrishnan, and C. von Keyserlingk, “Defining stable phases of open quantum systems,” (2024), [arXiv:2308.15495 \[quant-ph\]](#).
- [57] J. Y. Lee, W. Ji, Z. Bi, and M. P. A. Fisher, “Decoding measurement-prepared quantum phases and transitions: from ising model to gauge theory, and beyond,” (2022), [arXiv:2208.11699 \[cond-mat.str-el\]](#).
- [58] P.-S. Hsin, Z.-X. Luo, and H.-Y. Sun, “Anomalies of average symmetries: Entanglement and open quantum systems,” (2023), [arXiv:2312.09074 \[cond-mat.str-el\]](#).
- [59] S. Chirame, F. J. Burnell, S. Gopalakrishnan, and A. Prem, “Stable symmetry-protected topological phases in systems with heralded noise,” (2024), [arXiv:2404.16962](#).
- [60] Z. Li and R. S. K. Mong, “Replica topological order in quantum mixed states and quantum error correction,” (2024), [arXiv:2402.09516 \[quant-ph\]](#).
- [61] T. Ellison and M. Cheng, “Towards a classification of mixed-state topological orders in two dimensions,” (2024), [arXiv:2405.02390 \[cond-mat.str-el\]](#).
- [62] Y.-H. Chen and T. Grover, “Symmetry-enforced many-body separability transitions,” (2024), [arXiv:2310.07286 \[quant-ph\]](#).
- [63] Y.-H. Chen and T. Grover, [Phys. Rev. Lett.](#) **132**, 170602

- (2024).
- [64] Y. Zou, S. Sang, and T. H. Hsieh, *Phys. Rev. Lett.* **130**, 250403 (2023).
- [65] R. Fan, Y. Bao, E. Altman, and A. Vishwanath, *PRX Quantum* **5**, 020343 (2024).
- [66] S. Sang and T. H. Hsieh, “Stability of mixed-state quantum phases via finite markov length,” (2024), [arXiv:2404.07251 \[quant-ph\]](#).
- [67] Y.-H. Chen and T. Grover, “Unconventional topological mixed-state transition and critical phase induced by self-dual coherent errors,” (2024), [arXiv:2403.06553 \[quant-ph\]](#).
- [68] Z. Wang, Z. Wu, and Z. Wang, “Intrinsic mixed-state quantum topological order,” (2024), [arXiv:2307.13758 \[quant-ph\]](#).
- [69] R. Sohal and A. Prem, “A noisy approach to intrinsically mixed-state topological order,” (2024), [arXiv:2403.13879 \[cond-mat.str-el\]](#).
- [70] T.-C. Lu, “Disentangling transitions in topological order induced by boundary decoherence,” (2024), [arXiv:2404.06514 \[quant-ph\]](#).
- [71] J.-H. Zhang, K. Ding, S. Yang, and Z. Bi, *Phys. Rev. B* **108**, 155123 (2023).
- [72] Y. Guo, J.-H. Zhang, H.-R. Zhang, S. Yang, and Z. Bi, “Locally purified density operators for symmetry-protected topological phases in mixed states,” (2024), [arXiv:2403.16978 \[cond-mat.str-el\]](#).
- [73] H. Xue, J. Y. Lee, and Y. Bao, “Tensor network formulation of symmetry protected topological phases in mixed states,” (2024), [arXiv:2403.17069 \[cond-mat.str-el\]](#).
- [74] K. Su, N. Myerson-Jain, and C. Xu, *Phys. Rev. B* **109**, 035146 (2024).
- [75] N. Myerson-Jain, T. L. Hughes, and C. Xu, “Decoherence through ancilla anyon reservoirs,” (2023), [arXiv:2312.04638 \[cond-mat.str-el\]](#).
- [76] J. Y. Lee, “Exact calculations of coherent information for toric codes under decoherence: Identifying the fundamental error threshold,” (2024), [arXiv:2402.16937 \[cond-mat.stat-mech\]](#).
- [77] Z. Zhang, U. Agrawal, and S. Vijay, “Quantum communication and mixed-state order in decohered symmetry-protected topological states,” (2024), [arXiv:2405.05965 \[quant-ph\]](#).
- [78] Y. Guo and Y. Ashida, *Phys. Rev. B* **109**, 195420 (2024).
- [79] R. Masui and K. Totsuka, “Computational characterization of symmetry-protected topological phases in open quantum systems,” (2024), [arXiv:2405.18364 \[quant-ph\]](#).
- [80] C.-E. Bardyn and T. Karzig, *Phys. Rev. B* **94**, 094303 (2016).
- [81] Y.-J. Liu and S. Lieu, *Phys. Rev. A* **109**, 022422 (2024).
- [82] T. Iadecola, S. Ganeshan, J. H. Pixley, and J. H. Wilson, *Phys. Rev. Lett.* **131**, 060403 (2023).
- [83] M. Buchhold, T. Müller, and S. Diehl, “Revealing measurement-induced phase transitions by preselection,” (2022), [arXiv:2208.10506 \[cond-mat.dis-nn\]](#).
- [84] N. O’Dea, A. Morningstar, S. Gopalakrishnan, and V. Khemani, *Phys. Rev. B* **109**, L020304 (2024).
- [85] V. Ravindranath, Y. Han, Z.-C. Yang, and X. Chen, *Phys. Rev. B* **108**, L041103 (2023).
- [86] F. Arute, K. Arya, R. Babbush, D. Bacon, J. C. Bardin, R. Barends, R. Biswas, S. Boixo, F. G. Brandao, D. A. Buell, *et al.*, *Nature* **574**, 505 (2019).
- [87] A. Morvan, B. Villalonga, X. Mi, S. Mandrà, A. Bengtsson, P. V. Klimov, Z. Chen, S. Hong, C. Erickson, I. K. Drozdov, J. Chau, G. Laun, R. Movassagh, A. Asfaw, L. T. A. N. Brandão, R. Peralta, D. Abanin, R. Acharya, R. Allen, T. I. Andersen, K. Anderson, M. Ansmann, F. Arute, K. Arya, J. Atalaya, J. C. Bardin, A. Bilmes, G. Bortoli, A. Bourassa, J. Bovaird, L. Brill, M. Broughton, B. B. Buckley, D. A. Buell, T. Burger, B. Burkett, N. Bushnell, J. Campero, H. S. Chang, B. Chiaro, D. Chik, C. Chou, J. Cogan, R. Collins, P. Conner, W. Courtney, A. L. Crook, B. Curtin, D. M. Debroy, A. D. T. Barba, S. Demura, A. D. Paolo, A. Dunsworth, L. Faoro, E. Farhi, R. Fatemi, V. S. Ferreira, L. F. Burgos, E. Forati, A. G. Fowler, B. Foxen, G. Garcia, E. Genois, W. Gidney, C. Gidney, D. Gilboa, M. Giustina, R. Gosula, A. G. Dau, J. A. Gross, S. Habegger, M. C. Hamilton, M. Hansen, M. P. Harrigan, S. D. Harrington, P. Heu, M. R. Hoffmann, T. Huang, A. Huff, W. J. Huggins, L. B. Ioffe, S. V. Isakov, J. Iveland, E. Jeffrey, Z. Jiang, C. Jones, P. Juhas, D. Kafri, T. Khattar, M. Khezri, M. Kieferová, S. Kim, A. Kitaev, A. R. Klots, A. N. Korotkov, F. Kostritsa, J. M. Kreikebaum, D. Landhuis, P. Laptev, K. M. Lau, L. Laws, J. Lee, K. W. Lee, Y. D. Lensky, B. J. Lester, A. T. Lill, W. Liu, W. P. Livingston, A. Locharla, F. D. Malone, O. Martin, S. Martin, J. R. McClean, M. McEwen, K. C. Miao, A. Mieszala, S. Montazeri, W. Mruczkiewicz, O. Naaman, M. Neeley, C. Neill, A. Nersisyan, M. Newman, J. H. Ng, A. Nguyen, M. Nguyen, M. Y. Niu, T. E. O’Brien, S. Omonije, A. Opremcak, A. Petukhov, R. Potter, L. P. Pryadko, C. Quintana, D. M. Rhodes, E. Rosenberg, C. Rocque, P. Roushan, N. C. Rubin, N. Saei, D. Sank, K. Sankaragomathi, K. J. Satzinger, H. F. Schurkus, C. Schuster, M. J. Shearn, A. Shorter, N. Shutty, V. Shvarts, V. Sivak, J. Skrzynny, W. C. Smith, R. D. Somma, G. Sterling, D. Strain, M. Szalay, D. Thor, A. Torres, G. Vidal, C. V. Heidweiller, T. White, B. W. K. Woo, C. Xing, Z. J. Yao, P. Yeh, J. Yoo, G. Young, A. Zalcman, Y. Zhang, N. Zhu, N. Zobrist, E. G. Rieffel, R. Biswas, R. Babbush, D. Bacon, J. Hilton, E. Lucero, H. Neven, A. Megrant, J. Kelly, I. Aleiner, V. Smelyanskiy, K. Kechedzhi, Y. Chen, and S. Boixo, “Phase transition in random circuit sampling,” (2023), [arXiv:2304.11119 \[quant-ph\]](#).
- [88] L. Xiang, W. Jiang, Z. Bao, Z. Song, S. Xu, K. Wang, J. Chen, F. Jin, X. Zhu, Z. Zhu, F. Shen, N. Wang, C. Zhang, Y. Wu, Y. Zou, J. Zhong, Z. Cui, A. Zhang, Z. Tan, T. Li, Y. Gao, J. Deng, X. Zhang, H. Dong, P. Zhang, S. Jiang, W. Li, Z. Lu, Z.-Z. Sun, H. Li, Z. Wang, C. Song, Q. Guo, F. Liu, Z.-X. Gong, A. V. Gorshkov, N. Y. Yao, T. Iadecola, F. Machado, H. Wang, and D.-L. Deng, “Long-lived topological time-crystalline order on a quantum processor,” (2024), [arXiv:2401.04333 \[quant-ph\]](#).
- [89] A. Khindanov, Y.-X. Yao, and T. Iadecola, <https://doi.org/10.6084/m9.figshare.25979986> (2024).
- [90] K. Binder, *Z. Phys. B Con. Mat.* **43**, 119 (1981).
- [91] K. Binder, *Phys. Rev. Lett.* **47**, 693 (1981).
- [92] A. W. Sandvik, *AIP Conference Proceedings* **1297**, 135 (2010), [https://pubs.aip.org/aip/acp/article-pdf/1297/1/135/11407753/135-1\\_online.pdf](https://pubs.aip.org/aip/acp/article-pdf/1297/1/135/11407753/135-1_online.pdf).
- [93] The finite size crossing point here is slightly shifted from

- the value obtained from the large-system-size curves [depicted in Fig. 3(a)] due to a finite size drift caused by subleading terms in the Binder cumulant expansion near the critical point.
- [94] C. M. Bender and S. Boettcher, *Phys. Rev. Lett.* **80**, 5243 (1998).
  - [95] C. M. Bender, S. Boettcher, and P. N. Meisinger, *Journal of Mathematical Physics* **40**, 2201 (1999), [https://pubs.aip.org/aip/jmp/article-pdf/40/5/2201/19231175/2201\\_1\\_online.pdf](https://pubs.aip.org/aip/jmp/article-pdf/40/5/2201/19231175/2201_1_online.pdf).
  - [96] C. M. Bender, *Contemporary Physics* **46**, 277 (2005), <https://doi.org/10.1080/00107500072632>.
  - [97] A. A. Ovchinnikov, D. V. Dmitriev, V. Y. Krivnov, and V. O. Chervanskii, *Phys. Rev. B* **68**, 214406 (2003).
  - [98] For Trotter transitions in the context of quantum dynamics and information spreading, see Ref. [110–113].
  - [99] Y. Li and S. C. Benjamin, *Phys. Rev. X* **7**, 021050 (2017).
  - [100] I.-C. Chen, B. Burdick, Y.-X. Yao, P. P. Orth, and T. Iadecola, *Phys. Rev. Res.* **4**, 043027 (2022).
  - [101] A. Mari, N. Shammah, and W. J. Zeng, *Phys. Rev. A* **104**, 052607 (2021).
  - [102] E. van den Berg, Z. K. Mineev, A. Kandala, and K. Temme, *Nat. Phys.* **19**, 1116 (2023).
  - [103] B. McDonough, A. Mari, N. Shammah, N. T. Stemen, M. Wahl, W. J. Zeng, and P. P. Orth, in *2022 IEEE/ACM Third International Workshop on Quantum Computing Software (QCS)* (2022) pp. 83–93.
  - [104] G. Vidal, *Phys. Rev. Lett.* **91**, 147902 (2003).
  - [105] G. Vidal, *Phys. Rev. Lett.* **93**, 040502 (2004).
  - [106] D. C. Handscomb, *Mathematical Proceedings of the Cambridge Philosophical Society* **58**, 594–598 (1962).
  - [107] R. Blankenbecler and R. L. Sugar, *Phys. Rev. D* **27**, 1304 (1983).
  - [108] A. W. Sandvik and J. Kurkijärvi, *Phys. Rev. B* **43**, 5950 (1991).
  - [109] M. J. Beach, R. G. Melko, T. Grover, and T. H. Hsieh, *Phys. Rev. B* **100**, 094434 (2019).
  - [110] M. Heyl, P. Hauke, and P. Zoller, *Science Advances* **5**, eaau8342 (2019), <https://www.science.org/doi/pdf/10.1126/sciadv.aau8342>.
  - [111] L. M. Sieberer, T. Olsacher, A. Elben, M. Heyl, P. Hauke, F. Haake, and P. Zoller, *npj Quantum Information* **5**, 78 (2019).
  - [112] E. Vernier, B. Bertini, G. Giudici, and L. Piroli, *Phys. Rev. Lett.* **130**, 260401 (2023).
  - [113] P. Suchsland, R. Moessner, and P. W. Claeys, “Krylov complexity and trotter transitions in unitary circuit dynamics,” (2023), [arXiv:2308.03851 \[quant-ph\]](https://arxiv.org/abs/2308.03851).